

**Orbital angular momentum exchange in an optical parametric oscillator**M. Martinelli,<sup>1</sup> J. A. O. Huguenin,<sup>2</sup> P. Nussenzveig,<sup>1</sup> and A. Z. Khoury<sup>2,\*</sup><sup>1</sup>*Instituto de Física, Universidade de São Paulo, P.O. Box 66318, CEP 05315-970 São Paulo-SP, Brazil*<sup>2</sup>*Instituto de Física, Universidade Federal Fluminense, BR 24210-340, Niterói-RJ Brazil*

(Received 28 November 2003; published 28 July 2004)

We present a study of orbital angular momentum transfer from pump to down-converted beams in a type-II optical parametric oscillator. Cavity and anisotropy effects are investigated and demonstrated to play a central role in the transverse mode dynamics. While the idler beam can oscillate in a Laguerre-Gauss mode, the crystal birefringence induces an astigmatic effect in the signal beam that prevents the resonance of such a mode.

DOI: 10.1103/PhysRevA.70.013812

PACS number(s): 42.50.Lc, 42.65.Yj, 42.30.-d

**I. INTRODUCTION**

Early experiments have shown that circularly polarized light carries angular momentum [1]. In a quantum description of light, this angular momentum is associated with the spin of the photon. More recently significant attention has been given to the study of the orbital angular momentum of light, associated with phase singularities in the wave front. In a paraxial description of wave propagation, it is found that Laguerre-Gaussian beams carry orbital angular momentum. Such beams can be experimentally produced either by astigmatic mode conversion with cylindrical lenses [2,3], or by holographic techniques. In the latter, an optical beam is diffracted through amplitude [4–6] or phase masks [7] in order to produce the optical vortex. On one hand, amplitude masks can be easily produced with simple photographic techniques, but their use is quite limited when high power is required. On the other hand, the use of phase plates for high power operation requires delicate manufacturing techniques. Astigmatic mode converters can use simple optics (cylindrical lenses) to convert Hermite-Gauss into Laguerre-Gauss modes. They are also fairly suitable for high-power purposes, but require a high-order Hermite-Gauss mode to start with.

Many recent experiments have been performed to demonstrate the orbital angular momentum (OAM) conservation in nonlinear optical processes. It was observed in second harmonic generation [8,9], and a test of OAM conservation in parametric down conversion (PDC) was made by Arlt *et al.* [10], in the spontaneous regime. In the latter, no conservation was obtained in the macroscopic regime since the authors were detecting images of incoherent fields and hence were not sensitive to conservation properties of individual photon pairs. Clear evidence of OAM conservation in spontaneous PDC was obtained by Mair *et al.* [11], who observed entanglement between OAM variables of twin photons. In another experiment, Caetano *et al.* [12] introduced a stimulating beam, and parametric amplification was shown to be conditioned to OAM conservation.

So far, little attention has been given to OAM conservation in intracavity nonlinear coupling. Many studies have

been done with transverse multimode optical parametric oscillators (OPO's), showing interesting possibilities in pattern formation and quantum images for cavities with degenerate transverse modes, like planar [13,14] and spherical cavities [15,16]. Moreover, experiments have shown pattern formation in confocal [17] and concentric [18] cavities, and oscillation in modes with higher order than the fundamental are common in many different experiments [19,20].

Apart from theoretical studies on generation of phase singularities with nonlinear optical effects [21,22], only a few experimental results have been published on this subject, and to our knowledge, there is no result showing the necessary conditions for intracavity OAM transfer from the pump to the down-converted beams. In the present work, we study the OAM transfer in a nondegenerate, type-II optical parametric oscillator (OPO), operating above threshold. We show the conditions that must be satisfied for the OAM transfer, allowing one of the down-converted beams to oscillate with the same phase singularity of the pump beam. As we shall see, the astigmatism caused by the crystal birefringence plays a central role in the selection of the beam oscillating in the Laguerre-Gauss mode. However, under certain conditions, the OAM may be lost, and no phase singularity is observed in the down converted beams.

**II. EXPERIMENTAL SETUP AND RESULTS**

The experimental setup is shown in Fig. 1. The OPO is made by two spherical mirrors M1 and M2, with equal curvatures  $R_m = 13\text{mm}$ . Inside the cavity, we have a KTP crystal (by Cristal Laser) 10 mm long, cut for noncritical phase matching in 532–1064 nm down conversion at room temperature. In this case, the crystallographic axes ( $x, y, z$ ) of the crystal are oriented as follows. The  $z$  axis of the crystal is vertically oriented while the propagation direction lies on the horizontal plane ( $xy$ ). The  $x$  axis forms an angle  $\phi = 23.5^\circ$  with respect to the propagation direction.

The mirrors have high reflectance for the infrared ( $R = 99.8\%$  at 1064 nm), and a small transmittance at the pump wavelength ( $R = 92\%$  at 532 nm). Crystal losses in the infrared come mainly from surface reflection, reduced by antireflective coating ( $R = 0.1\%$ ), since crystal absorption at this wavelength is small (0.05%). For the pump, we have reflectance

---

\*Author to whom correspondence should be addressed; electronic address: khoury@if.uff.br

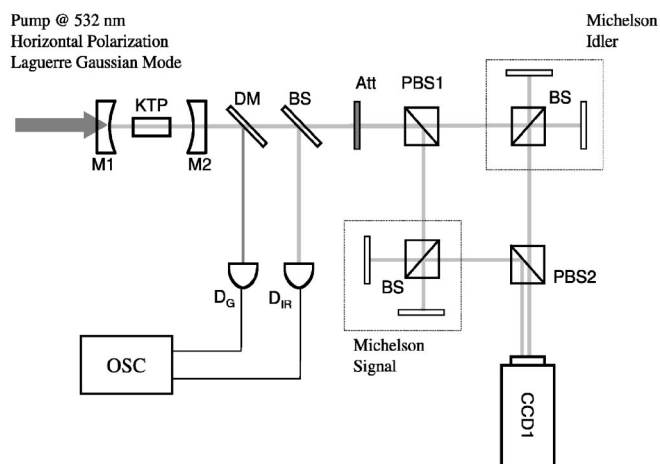


FIG. 1. Setup for the study of the phase singularities in the output of the type-II triply resonant OPO. The mode converter introduced in the pump beam is not shown.

tion losses ( $R=0.5\%$ ) and crystal absorption, increased by gray-tracking effects [23].

The cavity length is controlled by a piezoelectric actuator on the mirror, and the cavity is kept nearly confocal, in order to help the alignment and reduce the consequences of the walk off.

The OPO is pumped by the second harmonic of a Nd:YAG laser (Lightwave 142). This laser generates a  $TEM_{00}$  Gaussian beam, that is converted to a nearly Hermite-Gauss  $TEM_{01}$  beam [24]. With a telescope formed by two cylindrical lenses, we implemented a mode converter that produces a Laguerre-Gauss beam [2], with a good cylindrical symmetry for the intensity and a phase singularity in the center. This phase singularity was evidenced by the self-interference pattern obtained in a Michelson interferometer. In Fig. 2 we show the transverse profile and interference pattern of the beam used to pump the OPO. The resulting pump power is 60 mW. The beam is horizontally polarized, and mode matched to the cavity with the help of coated lenses.

Although the mirrors were high reflecting at 1064 nm, the output power coming out from the cavity through M2 can be detected by a PIN photodiode. The green light coming from the cavity is filtered by a dichroic mirror (DM), and detected by an amplified Si photodiode ( $D_G$ ). The infrared light is detected by a PIN InGaAs photodiode  $D_{IR}$  (ETX-300, from Epitaxx), that samples part of the output beam that is reflected by a beam splitter (BS).

In the output, signal and idler beams are separated by a polarizing cube (PBS). Adopting the usual convention in type-II OPO's, the idler beam polarization is horizontal, and the signal beam has a vertical polarization, aligned to the crystal  $z$  axis. Each down converted beam is sent into a Michelson interferometer made by a nonpolarizing 50/50 beam splitter (BS) and two flat mirrors, in order to produce interference fringes that can reveal the existence of a phase singularity. The two outputs are recombined in another polarizing cube (PBS) and sent onto a charge-coupled device (CCD) camera, that is used to register either the interference pattern or the intensity profile of the beam.

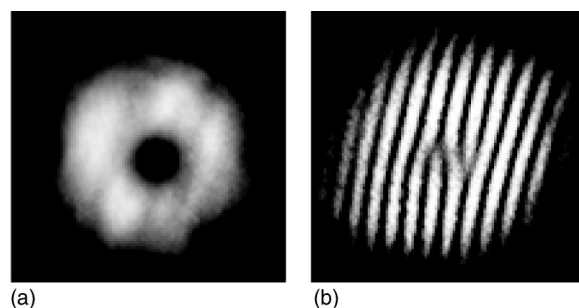


FIG. 2. (a) Transverse profile of the pump; (b) interference pattern showing the topological defects characteristic of phase singularities.

The output power of the pump and infrared beams is measured as the cavity length is scanned. The corresponding resonance peaks are shown in Fig. 3. A wide peak is obtained for the pump, over which narrow dips appear, owing to the pump depletion in different oscillation regimes. The resonance peaks for the infrared are also shown in Fig. 3. They coincide with the depletion dips in the pump resonance. Expanding the curve, we can observe that the depletion dips have a parabolic shape, in good agreement with the depletion expected for a triply resonant OPO [25]. From the finesse of the resonance peak for the pump, we measure 29% of internal losses in the cavity. For signal and idler modes, the fitting of the parabolic depletion gives a value of 1% for the infrared losses. The threshold power for parametric oscillation is around 20 mW.

The OPO could be kept oscillating, with a continuous output for as long as 10 min. In this situation, we registered the output image of signal and idler beams, as well as their self-interference patterns. These images are shown in Fig. 4. They are labeled in correspondence to the oscillation peaks shown in Fig. 3.

In images 1 and 4, the output intensity in the idler is the one of a Laguerre-Gauss beam. The corresponding interference patterns show the topological defects in the center of the Laguerre-Gauss beam characteristic of phase singularities. In this situation, the idler beam carries the orbital angular momentum of the down converted pump photons. In image 2, the shape of the idler beam is intermediary between a first order Laguerre-Gauss and a diagonal first-order Hermite-Gauss modes. A vortex can still be observed through the interference fringes. In both cases, the signal beam remains in the fundamental Gaussian mode. Following the Poincaré-sphere representation proposed in Ref. [26], we can look at the idler mode shown in image 2 as an orbital equivalent of an elliptical polarization.

An interesting effect appears in image 3. In this situation, the signal beam oscillates in the transverse mode with higher order, but with no angular momentum. The output is a pure Hermite-Gauss  $TEM_{01}$  mode, vertically oriented, while the idler remains in the fundamental Gaussian mode. Therefore the orbital angular momentum is not conserved in the parametric down conversion process, and the crystal is expected to suffer a twisting torque. This effect is analogous to the mechanical torque applied to a quarter wave plate used for light polarization conversion [1], or to a pair of cylindrical

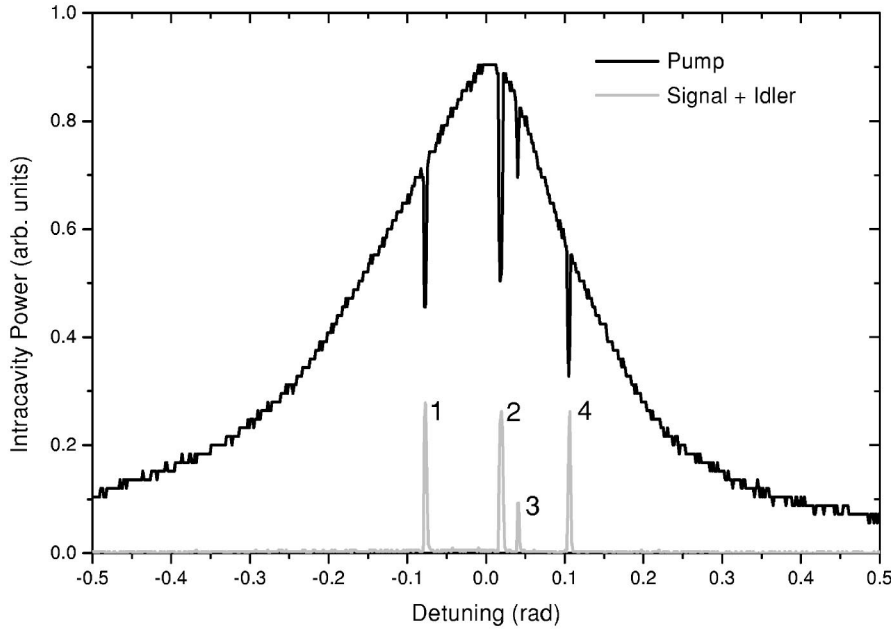


FIG. 3. Resonance peak for the pump beam, showing the oscillation of the OPO. The infrared peaks are labeled in order to identify the different images shown in Fig. 4.

lenses used for transverse-mode conversion [2].

The reason for this asymmetry in the OAM conservation of the pump can be explained when the propagation of paraxial beams in anisotropic media is investigated (see the Appendix). The resulting astigmatic cavity formed by the spherical mirrors and the anisotropic crystal will select the modes that will be able to oscillate.

### III. ASTIGMATIC CAVITY

As can be seen in the Appendix, when the effects of the crystal birefringence are taken into account, the paraxial

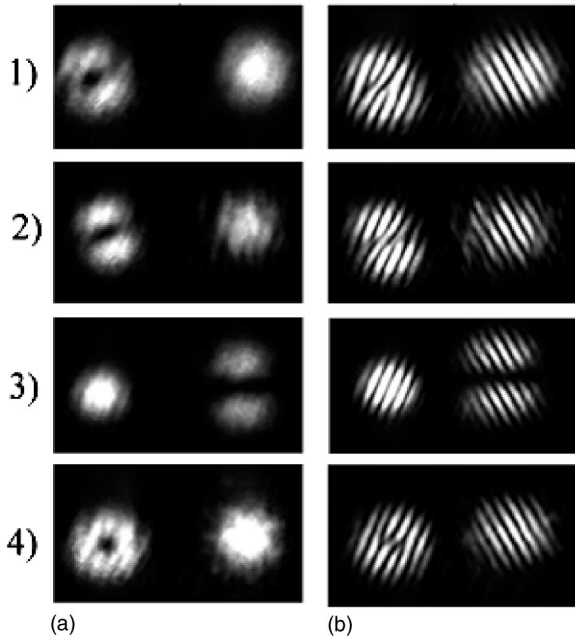


FIG. 4. (a) Intensity patterns for signal (right) and idler (left) beams labeled in correspondence with the infrared peaks shown in Fig. 3. (b) Self-interference patterns showing the presence or not of phase singularities.

wave equation for the propagating beams can be expressed with the help of rescaled spatial coordinates. All scaling parameters appearing in Eqs. (A13) and (A17) can be absorbed by a suitable definition of an effective wave number  $k_{eff}$  for each transverse direction and for each polarization. This brings Eqs. (A13) and (A17) to the general form

$$\partial_y^2 U(x, y) = 2ik_{eff} \partial_x U(x, y). \quad (1)$$

The normalized solution of Eq. (1) is [27]

$$U(x, y) = \left( \frac{k_{eff} x_R}{\pi 2^{2n} n!^2 (x^2 + x_R^2)} \right)^{1/4} H_n \left( y \sqrt{\frac{k_{eff} x_R}{x^2 + x_R^2}} \right) \times \exp \left[ -i \frac{k_{eff} y^2}{2(x + ix_R)} - i \left( n + \frac{1}{2} \right) \arctan \left( \frac{x}{x_R} \right) \right], \quad (2)$$

where  $x_R$  is the Rayleigh length, and  $H_n(x)$  is the Hermite polynomial of order  $n \geq 0$ . The term  $\arctan x/x_R$  is the well known Gouy phase shift. This term avoids multiple resonances of high-order Hermite-Gaussian (HG) modes in a high finesse cavity for the signal and idler modes of the OPO. The beam propagation is characterized by the beam waist  $w_0 = \sqrt{2x_R/k_{eff}}$  and the wave-front curvature  $R(x) = x(1 + x_R^2/x^2)$ . The change in the effective wave number is equivalent (in terms of beam diffraction) to the propagation in a shorter length of free space. Since the effective wave number depends both on polarization and transverse direction, we can consider a different propagation length in each case.

Let us now consider the refractive index of the KTP crystal at 1064 nm ( $n_x = 1.7404, n_y = 1.7479, n_z = 1.8296$ ) and 532 nm ( $n_x = 1.7797, n_y = 1.7897, n_z = 1.8877$ ), according to the manufacturer, Cristal Laser S.A. We have, for the extraordinary wave, a refractive index  $n(1064 \text{ nm}) = 1.7467$  and  $n(532 \text{ nm}) = 1.7881$ . From the distance  $L_0 = 17.4$  mm between the mirrors in our near-confocal cavity, and the crystal

length  $\ell = 10.0$  mm, we can calculate the effective length  $L$  of the cavity for each transverse mode, and for each polarization, in the infrared case. Using the relation

$$L = L_0 - \ell \frac{k_{eff} - k_0}{k_{eff}}, \quad (3)$$

we obtain, from the values of  $k_{eff}$  given by Eqs. (A13) and (A17)

$$\begin{aligned} L_{y'}^o &= 12.87 \text{ mm}, & L_z^o &= 13.40 \text{ mm}, & L_{y''}^e &= 13.17 \text{ mm}, \\ L_z^e &= 13.12 \text{ mm}, \end{aligned} \quad (4)$$

where the superscript  $o$  ( $e$ ) refers to the ordinary (extraordinary) wave. The effect of the walk off for the extraordinary wave has been taken into account, but the correction was  $\sim 10^{-4}$ , and could be neglected. The values of the Rayleigh length inside the cavity [ $x_R^2 = L^2(2R_m - L)/4$ ] for each transverse direction of the beam, and for each polarization, differ by less than 1%, and cannot be noticed in the free-propagating beam,

$$\begin{aligned} x_{Ry'}^o &= 6.500 \text{ mm}, & x_{Rz}^o &= 6.497 \text{ mm}, \\ x_{Ry''}^e &= 6.499 \text{ mm}, & x_{Rz}^e &= 6.500 \text{ mm}. \end{aligned} \quad (5)$$

On the other hand, the total Gouy phase shift accumulated in a round trip inside the cavity,  $\Phi = 4 \arctan(\sqrt{L}/\sqrt{2R_m - L})$ , will be

$$\begin{aligned} \Phi_{y'}^o &= 3.122 \text{ rad}, & \Phi_z^o &= 3.204 \text{ rad}, \\ \Phi_{y''}^e &= 3.167 \text{ rad}, & \Phi_z^e &= 3.161 \text{ rad}. \end{aligned} \quad (6)$$

The phase added in a round trip depends on the order of the Hermite-Gauss  $TEM_{mn}$  mode resonating inside the cavity. The total Gouy phase for this mode is

$$\Phi = (m + 1/2)\Phi_z + (n + 1/2)\Phi_y. \quad (7)$$

From the calculated values of the Gouy phase shift, we see that there will be a small phase difference between the  $TEM_{01}$  and the  $TEM_{10}$  modes. This difference will result in a splitting of the resonance position. At 1064 nm, this separation is of 82 mrad for the ordinary wave, and 6 mrad for the extraordinary one.

In order to study this splitting, we pumped the OPO with a Laguerre-Gaussian (LG) mode obtained with an astigmatic mode converter [2]. The LG mode is the superposition of two HG modes orthogonally oriented, that is, a  $TEM_{01}$  and a  $TEM_{10}$  mode. Once the OPO cavity is scanned, a single resonance peak is expected if the cavity is degenerate for the two TEM modes. Otherwise, two resonance peaks are expected, one corresponding to each TEM mode. In Fig. 5, we show the resonance peak of a high finesse cavity for a 532-nm LG pump. The polarization of the pump laser was rotated in order to provide both, the ordinary and extraordinary waves. For the vertical polarization (ordinary wave), a double resonance is observed as expected. This splitting shows a round trip phase difference of 88 mrad, in reasonable good agree-

ment with the predicted 93 mrad for 532 nm. On the other hand, for horizontal polarization (extraordinary wave), the LG resonance presents a single peak. In this case, the splitting is expected to be around 8 mrad, well below the resolution of the cavity used for this measurement.

From this analysis we conclude that the OPO can support the oscillation of an LG mode for the extraordinary wave, since its HG components have a degenerate (or quasidegenerate) resonance frequency. On the other hand, an LG mode in the ordinary wave cannot operate because its HG components will not have the same resonance frequency. This explains the results shown in Fig. 4, that is, the orbital angular momentum (OAM) is transferred from the pump laser (extraordinary wave) to the idler mode (extraordinary wave) but not to the signal mode (ordinary wave). Notice that, under our experimental conditions, only one of the down converted modes oscillates in a high-order transverse mode, while the other one oscillates in the fundamental transverse mode. So, the OAM exchange between pump, signal and idler modes is governed by the cavity dynamics under the crystal anisotropy, involving polarization and transverse profile aspects.

#### IV. THEORETICAL MODEL

Transverse multimode operation of OPO's has already been theoretically discussed in Ref. [28]. The pump beam can excite many different cavity modes for signal and idler, but in general it is the one with the lowest threshold that survives. Therefore modes with the best recovering integral should oscillate. To extend this description to our experiment, we must take into account the walk off and the astigmatism due to the crystal anisotropy. As we have seen, the astigmatism will introduce a phase shift between the two Hermite-Gauss components of the Laguerre-Gauss beam. We can choose to treat the problem either in the Laguerre-Gauss basis or in the Hermite-Gauss one. For the Laguerre-Gauss basis, the astigmatism couples the right-handed beam to the left-handed one. In the Hermite-Gauss basis, this coupling implies in a phase difference between the two first-order modes. Here we chose to work in the Hermite-Gauss basis, but the change of basis is straightforward.

In order to study the dynamics of the relevant transverse modes, we shall consider the normalized mode functions  $u_{jk}(x', y', z)$ , where  $j=p, s, i$  for pump, signal, and idler respectively, and  $k=0, h, v$  for the Hermite-Gauss  $TEM_{00}$ ,  $TEM_{10}$ , and  $TEM_{01}$ , respectively. The overlap integrals,

$$\begin{aligned} \Lambda_{klm} &= \int \int \int u_{pk}(x', y', z) u_{sl}^*(x', y', z) \\ &\quad \times u_{im}^*(x', y', z) dx' dy' dz, \end{aligned} \quad (8)$$

play an important role in the dynamics since they determine the transverse-mode coupling. The mode functions  $u_{jk}(x', y', z)$  are given by Eqs. (A13), (A17), and (2), where astigmatism and walk-off effects are taken into account. The walk off is slightly different for pump (4.1 mrad) and idler (3.2 mrad), and the significant astigmatism occurs in the  $z$  direction of the signal mode. The integrals are calculated in the whole crystal volume.

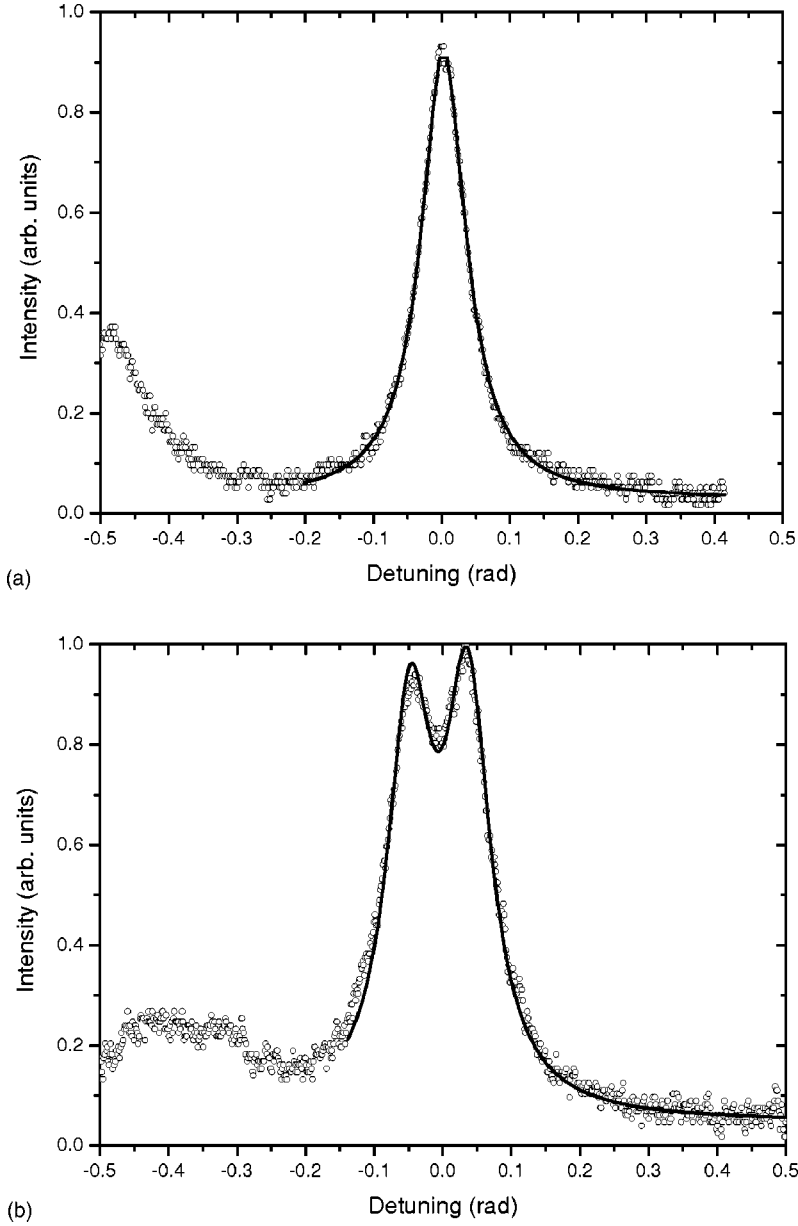


FIG. 5. Cavity resonance peak for a pump LG beam with (a) horizontal (extraordinary) polarization and (b) vertical (ordinary) polarization. In the second case the resonance peak splits in two, clearly showing the symmetry breaking between the two HG components of the LG beam.

With the overlap integrals, we can obtain the dynamic equations for the transverse-mode amplitudes. From all possible combinations of oscillating modes, the cavity parity will restrict the number of transverse modes for a given longitudinal mode. If there were no anisotropic effects, with a first order Laguerre-Gaussian pump mode, which is odd, signal and idler must have opposite parities in order to give a nonzero overlap integral. Therefore, for isotropic propagation, if signal oscillates in a first-order mode, idler must oscillate in the fundamental one, and vice versa. In principle, this parity selection breaks down for an anisotropic medium specially due to walk off. However, when the overlap integrals are calculated, we can see that the integrals for odd combinations of modes, like  $(v, 0, 0)$  or  $(v, v, v)$  for example, are indeed much smaller than those obtained with an even combination like  $(v, v, 0)$ . This allows us to neglect many of the mode couplings and restrict the number of dynamic equations. Two kinds of operation regimes are observed: either

the signal beam oscillates in the fundamental  $TEM_{00}$  mode, while the idler lies in the  $TEM_{01}$  and  $TEM_{10}$  subspace (peaks 1, 2, and 4 in Fig. 3), or the idler beam oscillates in the  $TEM_{00}$  mode (peak 3 in Fig. 3). Let us describe these regimes separately.

#### A. Signal beam operating in the $TEM_{00}$ mode

In this case, the set of dynamic equations for pump, signal, and idler transverse-mode amplitudes is

$$\dot{a}_{pv} = -[\gamma_p + i(\Delta_p + \sigma_p)]a_{pv} - i\chi\Lambda_{v0v}^* a_{s0} a_{iv} + E_{in}/\sqrt{2},$$

$$\dot{a}_{ph} = -[\gamma_p + i(\Delta_p - \sigma_p)]a_{ph} - i\chi\Lambda_{h0h}^* a_{s0} a_{ih} - i E_{in}/\sqrt{2},$$

$$\dot{a}_{s0} = -(\gamma + i\Delta_s)a_{s0} + i\chi\Lambda_{v0v} a_{pv} a_{iv}^* + i\chi\Lambda_{h0h} a_{ph} a_{ih}^*,$$

$$\dot{a}_{iv} = -[\gamma + i(\Delta_i + \sigma_i)]a_{iv} + i\chi\Lambda_{v0v} a_{pv} a_{s0}^*,$$

$$\dot{a}_{ih} = -[\gamma + i(\Delta_i - \sigma_i)]a_{ih} + i\chi\Lambda_{h0h}a_{ph}a_{s0}^*, \quad (9)$$

where the subindexes  $p$ ,  $s$ , and  $i$  refer to pump, signal, and idler respectively, and  $0$ ,  $v$ , and  $h$  refer to fundamental (TEM<sub>00</sub>), vertical (TEM<sub>01</sub>), and horizontal (TEM<sub>10</sub>) transverse modes. Pump losses are described by  $\gamma_p$  while a common decay rate  $\gamma$  represents the losses for signal and idler. The respective cavity detunings for pump, signal, and idler are  $\Delta_p$ ,  $\Delta_s$ , and  $\Delta_i$ . The astigmatic symmetry breaking is accounted for through the frequency splitting parameters  $\sigma_p$  for pump and  $\sigma_i$  for idler. They are calculated with the help of Eq. (7). The pump beam amplitude transmitted through the input mirror is represented by the source term  $E_{in}$ . Since it is prepared in a Laguerre-Gauss mode, the source terms appearing in the dynamic equations for the amplitudes  $a_{pv}$  and  $a_{ph}$  are  $\pi/2$  out of phase. Finally,  $\chi$  is the nonlinear coupling constant.

The dynamic equations, as well as their steady-state solutions, are considerably simplified if we express time in units of the cavity round-trip time  $\tau$  and define the following normalized variables:

$$\begin{aligned} b_{jk} &= \chi\Lambda_{000}\tau a_{jk}, & x_{in} &= \chi\Lambda_{000}\tau^2 E_{in}, \\ \tilde{\gamma}_j &= \gamma_j\tau, & \tilde{\Delta}_j &= \Delta_j\tau, & \tilde{\sigma}_j &= \Delta_j\tau, \\ \eta_{klm} &= \frac{\Lambda_{klm}}{\Lambda_{000}}. \end{aligned} \quad (10)$$

As before,  $j=p,s,i$  for pump, signal, and idler, respectively, and each of the subindexes  $k$ ,  $l$ , and  $m$  may assume the values  $0$ ,  $h$ , or  $v$ . Cavity losses are around 29% at 532 nm and 1% at 1064 nm that give  $\tilde{\gamma}_p=145$  mrad and  $\tilde{\gamma}=5$  mrad. In the absence of astigmatism and walk off the relevant normalized overlap integrals are  $\eta_{vv0}=\eta_{hh0}=\eta_{v0v}=\eta_{h0h}=0.71$  approximately. When the walk-off effect is considered, the overlap integrals are averaged over the crystal volume. Moreover, the astigmatism is included through the appropriate correction of the mode functions. Taking into account the experimental values for the walk-off and astigmatism parameters we find  $\eta_{vv0}=0.70$ ,  $\eta_{hh0}=0.60$  and  $\eta_{v0v}\approx\eta_{h0h}\approx 0.71$ . So, a significant change is obtained only for  $\eta_{hh0}$ .

It is instructive to consider the steady-state solution of Eqs. (9) in the simplified condition  $\Delta_s=\Delta_i=\sigma_p=\sigma_i=0$  and  $\eta_{v0v}=\eta_{h0h}=\eta$  which correspond to neglecting walk off and astigmatism. In this case the orbital angular momentum is perfectly transferred to the idler beam which will also oscillate in a Laguerre-Gauss mode with the same topological charge of the pump beam. Therefore the steady-state solutions are

$$\begin{aligned} I_{p-} &= I_{i-} = 0, & I_{p+} &= \tilde{\gamma}^2/\eta^2, \\ I_{s0} &= I_{i+} = I_0 = \frac{\tilde{\gamma}}{\eta^2} \left[ \sqrt{\frac{\eta^2 x_{in}^2}{\tilde{\gamma}^2} - \tilde{\Delta}_p^2 - \tilde{\gamma}_p} \right], \end{aligned} \quad (11)$$

where we defined the normalized intensities  $I_{jk}=|b_{jk}|^2$ . The Laguerre-Gauss amplitudes  $b_{j\pm}$  are given in terms of the Hermite-Gauss amplitudes as

$$b_{j\pm} = \frac{b_{jv} \pm ib_{jh}}{\sqrt{2}}. \quad (12)$$

The threshold value of  $x_{in}$  for parametric oscillation is obtained by setting  $I_0=0$  so that

$$x_L^2 = \frac{\tilde{\gamma}^2}{\eta^2} (\tilde{\gamma}_p^2 + \tilde{\Delta}_p^2). \quad (13)$$

As we shall see, a different threshold condition is obtained for the other operation regime, in which the idler beam operates in the TEM<sub>00</sub> mode.

The analytical solution for the steady state including all parameters is cumbersome but Eqs. (11) give us a good estimate for the orders of magnitude. In fact, as we discussed in Sec. IV, the expected value for the pump and idler splitting parameters are indeed very small,  $\tilde{\sigma}_p=4$  mrad and  $\tilde{\sigma}_i=3$  mrad [the splitting parameter is half the astigmatic phase shift calculated from Eq. (7)]. However, this small splitting may be responsible for partial transfer of the orbital angular momentum from the pump to the idler mode. In order to illustrate this, we numerically integrated the dynamic equations (9) with a fourth-order Runge-Kutta method until the steady state was reached. In Fig. 6 this time evolution is shown together with the value  $I_0$  given by Eq. (11). In the inset, we show the expected image for signal (S) and idler (I) obtained with the numerical steady-state results. A good qualitative agreement is obtained with the experimental results corresponding to peaks 1, 2, and 4 of Fig. 3.

### B. Idler beam operating in the TEM<sub>00</sub> mode

In this case the dynamic equations are

$$\begin{aligned} \dot{a}_{pv} &= -[\gamma_p + i(\Delta_p + \sigma_p)]a_{pv} - i\chi\Lambda_{vv0}^* a_{sv} a_{i0} + E_{in}/\sqrt{2}, \\ \dot{a}_{ph} &= -[\gamma_p + i(\Delta_p - \sigma_p)]a_{ph} - i\chi\Lambda_{hh0}^* a_{sh} a_{i0} - i E_{in}/\sqrt{2}, \\ \dot{a}_{sv} &= -[\gamma + i(\Delta_s + \sigma_s)]a_{sv} + i\chi\Lambda_{vv0} a_{pv} a_{i0}^*, \\ \dot{a}_{sh} &= -[\gamma + i(\Delta_s - \sigma_s)]a_{sh} + i\chi\Lambda_{hh0} a_{ph} a_{i0}^*, \\ \dot{a}_{i0} &= -(\gamma + i\Delta_i)a_{i0} + i\chi\Lambda_{vv0} a_{pv} a_{sv}^* + i\chi\Lambda_{hh0} a_{ph} a_{sh}^*. \end{aligned} \quad (14)$$

The transverse-mode splitting now appears in the dynamic equation for the signal beam and is represented by the parameter  $\sigma_s$ . However, the splitting parameter is expected to be of the order of 41 mrad. Since cavity losses in the infrared are of the order of 1%, the corresponding normalized decay rate is  $\tilde{\gamma}=5$  mrad, so that  $\sigma_s \gg \tilde{\gamma}$ . Under such conditions it is impossible for the OPO to support the simultaneous operation of the  $h$  and  $v$  modes necessary to compose a Laguerre-Gauss mode. Therefore the orbital angular momentum cannot be transferred to the down-converted beams. The cavity tuning will select the signal Hermite-Gauss mode whose resonance frequency is closer to the idler resonance. For example, for  $\Delta_s=-\sigma_s$  the cavity frequency falls far away from the  $h$  signal resonance while the  $v$  mode gets on resonance. In this case  $a_{sh}\approx 0$  and the steady-state solution of Eqs. (14)

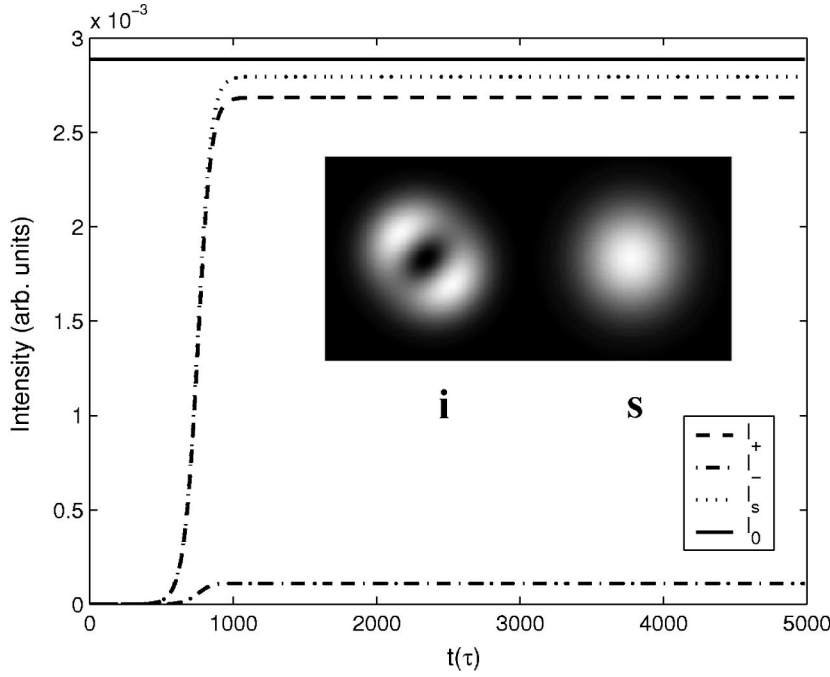


FIG. 6. Time evolution of the down-converted beam intensities (in units of the cavity round-trip time) obtained from numerical integration of the dynamic equations (9). The inset shows the corresponding expected images for signal (s) and idler (i). The parameter values used are  $\Delta_p=0.071\gamma_p$ ,  $\Delta_s=0$ ,  $\Delta_i=1$  mrad,  $\gamma_p=145$  mrad,  $\gamma=5$  mrad,  $\sigma_p=4$  mrad,  $\sigma_i=3$  mrad,  $x_{in}=3x_L$ , and  $\eta_{v0v}=\eta_{h0h}=0.71$ . The horizontal solid line shows the analytical value  $I_0$ .

can be analytically obtained. Notice that the normalized overlap integral  $\eta_{hh0}$  will not play any role in this case. We therefore set  $\eta=\eta_{v0v}$  and use the same normalizations adopted in Eqs. (10) to find

$$I_{sh}=0, \quad I_{ph}=\frac{x_{in}^2/2}{\tilde{\gamma}_p^2+\tilde{\Delta}_p^2}, \quad I_{pv}=\frac{\tilde{\gamma}^2}{\eta^2},$$

$$I_{i0}=I_{sv}=I'_0=\frac{\tilde{\gamma}}{\eta^2}\left[\sqrt{\frac{\eta^2 x_{in}^2}{2\tilde{\gamma}^2}-\tilde{\Delta}_p^2}-\tilde{\gamma}_p\right]. \quad (15)$$

The  $h$  component of the pump beam does not couple to the down-converted modes so that its steady-state solution cor-

responds just to an empty cavity. On the other hand, the  $v$  component of the signal beam, as well as the fundamental idler mode, presents a steady-state intensity lower than the one found in Eqs. (11) for the same pump level  $x_{in}$ . This corresponds to the situation found in peak 3 of Fig. 3, which is clearly lower than the other infrared peaks. Again, the oscillation threshold is readily obtained by taking  $I'_0=0$ :

$$x_L^2=\frac{2\tilde{\gamma}^2}{\eta^2}(\tilde{\gamma}_p^2+\tilde{\Delta}_p^2). \quad (16)$$

It is twice the threshold value for the case where the orbital angular momentum is transferred for the idler beam, what is

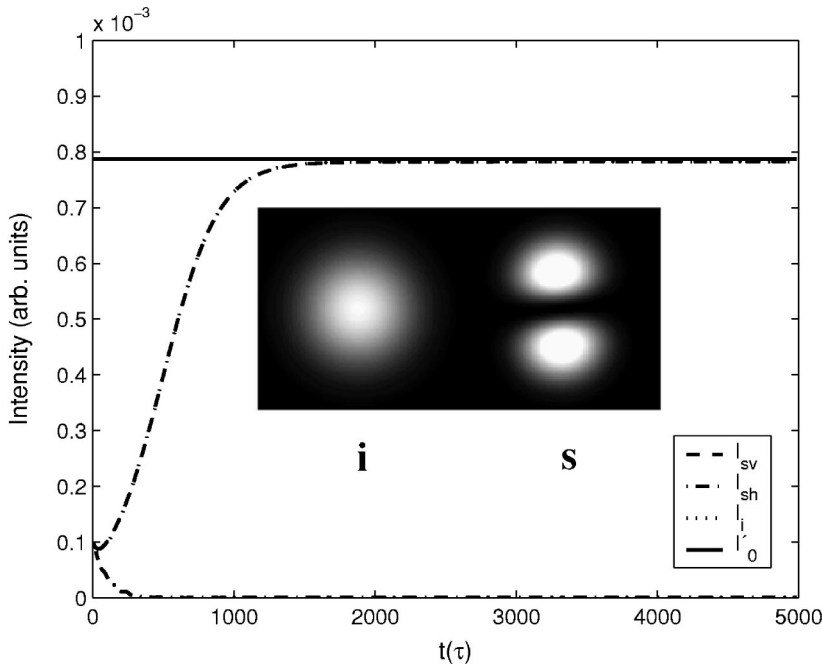


FIG. 7. Time evolution of the down-converted beam intensities (in units of the cavity round-trip time) obtained from numerical integration of the dynamic equations (14). The inset shows the corresponding expected images for signal (s) and idler (i). The parameter values used are  $\Delta_p=0.28\gamma_p$ ,  $\Delta_s=-41$  mrad,  $\Delta_i=0$ ,  $\gamma_p=145$  mrad,  $\gamma=5$  mrad,  $\sigma_p=4$  mrad,  $\sigma_s=41$  mrad,  $x_{in}=1.5x_L$ , and  $\eta_{v0v}=0.70$ . The horizontal solid line shows the analytical value  $I'_0$ .

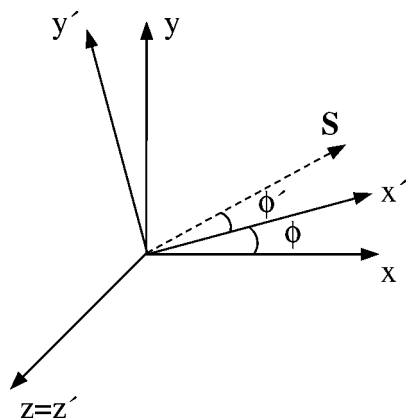


FIG. 8. Coordinate system used to describe the paraxial propagation through the anisotropic crystal. The walk-off angle  $\phi'$  is indicated as the angle between the Poynting vector  $\mathbf{S}$  and the propagation axis  $x'$ .

also coherent with the lower height of peak 3 in Fig. 3.

The numerical evolution of Eqs. (14) using a fourth order Runge-Kutta method was performed without the simplifying assumptions. These results are presented in Fig. 7, where the inset shows the expected images for signal and idler. The walk-off and astigmatic effects were fully considered and a good agreement with the experimental result was obtained.

## V. CONCLUSION

We have shown that the transfer of orbital angular momentum in intracavity parametric down conversion is strongly subjected to cavity and anisotropy effects. Orbital angular momentum conservation can be observed only if pump, signal, and idler are in a set of modes where the Hermite-Gauss (HG) components of the Laguerre-Gauss (LG) modes are degenerate inside the cavity. While that can be easily achieved for the idler beam, the signal beam cannot fulfill this condition unless cavity losses are large. If the idler beam oscillates in the fundamental mode, one can still obtain signal oscillation in a higher transverse mode. However, since the HG components are not degenerate, the threshold power increases, and the orbital angular momentum is not transferred to the down-converted beams.

We also developed a theoretical model, which presents good agreement with the experimental results, and which should be useful for future investigations of the transverse-mode dynamics in the quantum domain. Interesting perspectives can be envisaged if the OPO operation is subject to an injected signal. Recent studies on degenerate [29] and non-degenerate [30] parametric processes with injected signal have considered interesting issues such as the preparation of quantum correlated states (Einstein-Podolsky-Rosen states), as well as the study of critical behaviors of the OPO operation [31].

## ACKNOWLEDGMENTS

A. Z. K. thanks Professor D. Petrov for bringing the optical vortices to his attention during the Jorge André Swieca

Summer School on Quantum and Nonlinear Optics at Recife, Brazil. We also thank C. H. Monken and A. G. C. Moura for fruitful discussions regarding the propagation of optical beams in anisotropic media. Funding was provided by Fundação de Amparo à Pesquisa do Estado de São Paulo (FAPESP-BR), Coordenação de Aperfeiçoamento de Pessoal de Nível Superior (CAPES/PROCAD and CAPES/COFECUB projects), Fundação de Amparo à Pesquisa do Estado do Rio de Janeiro (FAPERJ-BR), and Conselho Nacional de Desenvolvimento Científico e Tecnológico (CNPq) through the *Instituto do Milênio de Informação Quântica*.

## APPENDIX: PARAXIAL WAVES IN A BIREFRINGENT CRYSTAL

In a type-II down-conversion, we use the crystal birefringence to achieve the desired phase matching condition [32,33]. It was shown by many authors that the paraxial equation, from which we can derive the propagation modes of a beam in free space or isotropic medium, will change when we work with an anisotropic medium [34,35]. Here we will extend the study of Fleck and Feit [36] of paraxial propagation in uniaxial crystals to the biaxial case, adapting their description to the case of a crystal inside a cavity. Our aim is to reduce the wave equations to the paraxial wave equations that define the Hermite-Gauss modes coupled to the resonances of a linear cavity.

Let us define the crystallographic axes as  $(x, y, z)$ . The KTP crystal used in our experiment is a quasiuniaxial one with  $n_x \sim n_y \neq n_z$ , where  $n_{x(y,z)}$  is the refraction index for  $x(y, z)$  polarized light. Since the displacement vector  $\mathbf{D}$  satisfies  $\nabla \cdot \mathbf{D} = 0$ , we can write the wave equation for the electric field  $\mathbf{E}$ , derived from Maxwell's equations, as

$$\nabla^2 \mathbf{E} - \nabla \left( \nabla \cdot \mathbf{E} - \frac{\nabla \cdot \mathbf{D}}{\alpha} \right) + k_0^2 \boldsymbol{\varepsilon} \cdot \mathbf{E} = 0, \quad (\text{A1})$$

where  $k_0 = \omega/c$  is the wave number in vacuum corresponding to frequency  $\omega$ , and  $\alpha$  is a constant to be conveniently chosen. This constant will significantly simplify the paraxial propagation analysis in the birefringent medium. The constitutive relation  $\mathbf{D} = \boldsymbol{\varepsilon} \cdot \mathbf{E}$  depends on the dielectric tensor  $\boldsymbol{\varepsilon}$ , that is diagonal when we use the crystallographic coordinates

$$\boldsymbol{\varepsilon} = \begin{bmatrix} n_x^2 & 0 & 0 \\ 0 & n_y^2 & 0 \\ 0 & 0 & n_z^2 \end{bmatrix}. \quad (\text{A2})$$

The wave equations for the electric field components can be derived from Eq. (A1) by using the constitutive relation and choosing  $\alpha = n_y^2$  to obtain

$$\begin{aligned} \frac{n_x^2}{n_y^2} \partial_x^2 E_x + \partial_y^2 E_x + \partial_z^2 E_x - \left( 1 - \frac{n_x^2}{n_y^2} \right) \partial_x \partial_z E_z + k_0^2 n_x^2 E_x &= 0, \\ \partial_x^2 E_y + \partial_y^2 E_y + \partial_z^2 E_y - \left( 1 - \frac{n_x^2}{n_y^2} \right) \partial_y \partial_x E_x - \left( 1 - \frac{n_z^2}{n_y^2} \right) \partial_y \partial_z E_z \\ + k_0^2 n_y^2 E_y &= 0, \end{aligned}$$

$$\partial_x^2 E_z + \partial_y^2 E_z + \frac{n_z^2}{n_y^2} \partial_z^2 E_z - \left(1 - \frac{n_x^2}{n_y^2}\right) \partial_z \partial_x E_x + k_0^2 n_z^2 E_z = 0. \quad (\text{A3})$$

Notice that for a uniaxial crystal ( $n_x = n_y$ ) we recover the equations obtained in Ref. [36]. Let us now consider propagation along an axis  $x'$  lying on the  $xy$  plane with an angle  $\phi$  with respect to the crystallographic axis  $x$ , as shown in Fig. 8. This definition of  $\phi$  has the advantage to match the angle and axis definitions usually given by crystal manufacturers. For our KTP crystal, cut for type-II phase matching of 532 and 1064 nm, we have  $\phi = 23.5^\circ$ . A rotated reference frame ( $x', y', z$ ) can be used to describe the propagation inside the crystal. The coordinate transformation between the two frames is

$$\begin{aligned} x' &= x \cos \phi + y \sin \phi, \\ y' &= -x \sin \phi + y \cos \phi, \\ z' &= z. \end{aligned} \quad (\text{A4})$$

### 1. Plane-wave analysis

Two orthogonally polarized plane-wave solutions propagating along  $x'$  can be found for Eqs. (A3), one with  $E_x = E_y = 0$  and  $E_z \neq 0$  ( $z$  polarized) and another polarized in the  $xy$  plane ( $E_z = 0$ ). For the  $z$  polarized solution, only the last of Eqs. (A3) remain and its solution is

$$E_z = E_{0z} e^{in_z k_0 x'}. \quad (\text{A5})$$

The plane-wave solution polarized on the  $xy$  plane can be found by making  $E_z = 0$  in the first two of Eqs. (A3). This solution is of the kind

$$\mathbf{E} = \mathbf{E}_0 e^{i(k_x x + k_y y)}, \quad (\text{A6})$$

where  $\mathbf{E}_0 = E_{0x} \hat{x} + E_{0y} \hat{y}$ . From substitution of Eq. (A6) in the first one of Eqs. (A3), we find

$$\frac{k_x^2}{n_y^2} + \frac{k_y^2}{n_x^2} = k_0^2, \quad (\text{A7})$$

which is the projection of the well-known index ellipsoid on the  $xy$  plane. By making  $k_x = n k_0 \cos \phi$  and  $k_y = n k_0 \sin \phi$ , we get

$$\frac{\cos^2 \phi}{n_y^2} + \frac{\sin^2 \phi}{n_x^2} = \frac{1}{n^2}, \quad (\text{A8})$$

where  $n$  is the index of refraction for propagation along  $x'$ . On the other hand, if we substitute Eq. (A6) in the constitutive relation  $\mathbf{D} = \boldsymbol{\varepsilon} \cdot \mathbf{E}$  and in  $\nabla \cdot \mathbf{D} = 0$  we find that

$$n_x^2 k_x E_x + n_y^2 k_y E_y = 0. \quad (\text{A9})$$

Since  $n_x \neq n_y$ , this means that  $\mathbf{E}$  and  $\mathbf{k}$  are not orthogonal. Therefore the Poynting vector  $\mathbf{S}$ , that is orthogonal to  $\mathbf{E}$ , is not parallel to  $\mathbf{k}$ . Let us call  $\phi'$  the angle between  $\mathbf{S}$  and  $\mathbf{k}$ . A straightforward geometric analysis allows one to obtain a simple relation between  $\phi$  and  $\phi'$ :

$$\tan \phi' = \frac{\sin \phi \cos \phi (n_y^2 - n_x^2)}{n_x^2 \cos^2 \phi + n_y^2 \sin^2 \phi}. \quad (\text{A10})$$

This angle is represented in Fig. 8. It is related to the well-known walk-off effect, which appears as a consequence of the crystal anisotropy. However, as we shall see shortly, the  $z$  polarized field will also have an anisotropic effect when the propagation of a transversely finite beam is considered. This effect appears as an astigmatic deformation of the beam during the propagation along the crystal.

### 2. Paraxial propagation

On the other hand, to obtain a direct solution of Eq. (A1) for a paraxial beam propagation is not so straightforward and some careful approximations have to be made to uncouple the differential equations for each polarization. For the  $z$  component, the wave equation has the form

$$\begin{aligned} \left( \partial_x^2 + \partial_y^2 + \frac{n_z^2}{\alpha} \partial_z^2 + k_0^2 n_z \right) E_z - \left( \frac{\alpha - n_x^2}{\alpha} \right) \partial_x \partial_z E_x \\ - \left( \frac{\alpha - n_y^2}{\alpha} \right) \partial_y \partial_z E_y = 0. \end{aligned} \quad (\text{A11})$$

To reduce this equation to the paraxial wave equation for  $z$  polarization, we can begin by eliminating the terms with cross derivatives. One way to do this is to approximate the biaxial crystal by a uniaxial one for the  $z$  polarization. This is valid since  $|n_x - n_y| \ll |n_z - n_y|$ . If we chose  $\alpha = n^2$ , we have  $|(\alpha - n_i^2)/\alpha| \cong 10^{-2}$  for  $i = \{x, y\}$ , giving a very small contribution. In the limit  $n_x = n_y = n$  these terms will vanish, and we have the uniaxial crystal studied in Ref. [36].

A paraxial solution  $E_z = u_z(x', y', z) e^{-in_z k_0 x'}$  of Eq. (A11) can be obtained if we adopt the rotated reference frame. The resulting equation is close to the paraxial wave equation, except for the asymmetry in the coefficients of the transverse second-order derivatives:

$$\partial_y^2 u_z + \frac{n_z^2}{n^2} \partial_z^2 u_z = 2in_z k_0 \partial_x u_z. \quad (\text{A12})$$

The asymmetry between the transverse coordinates  $y'$  and  $z$  appears as a rescaling of the  $z$  coordinate. This means that the optical beam follows an astigmatic propagation inside the crystal with different diffraction scales for each transverse coordinate. Let us separate the dependence of  $u_z$  on  $y'$  and  $z$  making  $u_z(x', y', z) = U_z(x', y') V_z(x', z)$ , in order to obtain two paraxial wave equations for the beam diffraction in each transverse direction:

$$\partial_y^2 U_z = 2in_z k_0 \partial_x U_z,$$

$$\frac{n_z^2}{n^2} \partial_z^2 V_z = 2in_z k_0 \partial_x V_z. \quad (\text{A13})$$

When calculating the propagation of the beam through an OPO cavity, this diffraction asymmetry can be seen as a different effective length of the crystal for each transverse dependence of the mode function. For a crystal with length  $\ell$ ,

the effective length for the  $U_z$  propagation will be  $\ell/n_z$ , as usual in the treatment of beam propagation through a uniform crystal [28,33]. For  $V_z$ , the effective length it will be  $\ell n_z/n^2$ , resulting in an asymmetry in the effective cavity length for each transverse evolution. The calculation of the cavity geometry, and the resulting beam parameters expressed by the Rayleigh length  $x_R$ , will therefore differ for the two transverse coordinates.

Let us now turn to the paraxial solution for the field polarized on the  $xy$  plane. Since a plane-wave solution with  $E_z=0$  can be found, it is natural to conceive a paraxial solution for which  $E_z$  is negligible. Therefore if we choose  $\alpha = n_x^2$  in Eq. (A1) and use the rotated coordinates, we obtain the following propagation equation for  $E_y$ :

$$\left[ \cos^2\phi \partial_{x'}^2 + \sin^2\phi \partial_{y'}^2 - \sin 2\phi \partial_{x'}\partial_{y'} + \frac{n_y^2}{n_x^2}(\sin^2\phi \partial_{x'}^2 + \cos^2\phi \partial_{y'}^2 + \sin 2\phi \partial_{x'}\partial_{y'}) + \partial_z^2 + k_0^2 n_y \right] E_y = 0. \quad (\text{A14})$$

We now try a paraxial solution of the form  $E_y = u_y(x', y', z)e^{-ink_0 x'}$  in Eq. (A14), using Eq. (A8) and making the paraxial approximation to obtain

$$2ik_0 n_y \left( \cos^2\phi + \frac{n_y^2}{n_x^2} \sin^2\phi \right)^{1/2} [\partial_{x'} u_y + \tan\phi' \partial_{y'} u_y] = \left( \sin^2\phi + \frac{n_y^2}{n_x^2} \cos^2\phi \right) \partial_{y'}^2 u_y + \partial_z^2 u_y, \quad (\text{A15})$$

where  $\phi'$  is the walk-off angle given by Eq. (A10). In order to obtain a paraxial wave equation, a second coordinate

transformation  $y'' = y' - \tan\phi' x'$  is necessary. This transformation corresponds to a transverse offset of the  $xy$  polarized beam. Using Eq. (A8) and defining  $\xi^2 = \sin^2\phi + (n_y^2/n_x^2)\cos^2\phi$ , we can rewrite Eq. (A15) as

$$2ik_0 \frac{n_y^2}{n} \partial_{x'} u_y = \xi^2 \partial_{y''}^2 u_y + \partial_z^2 u_y, \quad (\text{A16})$$

that is, the usual paraxial equation with wave vector  $k_0(n_y^2/n)$  and a rescaled transverse coordinate  $y''/\xi$ . However, since  $n_x \sim n_y$ , this transverse rescaling is much smaller than the one present in the  $z$  polarized field. Therefore, while the  $z$  polarization has a significant astigmatism but no walk off, the  $xy$  polarization presents walk off and a small astigmatism. From now on we shall designate the  $xy$  polarized field as the *extraordinary* wave and the  $z$  polarized field as the *ordinary* wave.

As we made for the  $z$  component, we can try a factorized solution of the paraxial wave equation (A16) of the form  $u_y = U_y(x', y'')V_y(x', z)$ , so that

$$\xi^2 \partial_{y''}^2 U_y = 2ik_0 (n_y^2/n) \partial_{x'} U_y, \quad \partial_z^2 V_y = 2ik_0 (n_y^2/n) \partial_{x'} V_y. \quad (\text{A17})$$

Thus the paraxial propagation inside the crystal is well described by Eqs. (A13) and (A17) for the ordinary and extraordinary waves, respectively. A paraxial equation for the  $x$  component of the extraordinary wave can be obtained on the same lines leading to Eq. (A17).

- 
- [1] R. A. Beth, Phys. Rev. **50**, 115 (1936).  
 [2] M. W. Beijersbergen, L. Allen, H. E. L. O. var der Veen, and J. P. Woerdman, Opt. Commun. **96**, 123 (1992).  
 [3] E. Abramochkin and V. Volostnikov, Opt. Commun. **83**, 123 (1991).  
 [4] N. R. Heckenberg, R. McDuff, C. P. Smith, and A. G. White, Opt. Lett. **17**, 221 (1992).  
 [5] G. F. Brand, Am. J. Phys. **67**, 55 (1999).  
 [6] J. A. O. Huguenin, B. Coutinho dos Santos, P. A. M. dos Santos, and A. Z. Khoury, J. Opt. Soc. Am. A **20**, 1883 (2003).  
 [7] S. S. R. Oemrawsingh, J. A. W. van Houwelingen, E. R. Eliel, J. P. Woerdman, E. J. K. Verstegen, J. G. Kloosterboer, and G. W. 't Hooft, Appl. Opt. **43**, 688 (2004).  
 [8] K. Dholakia, N. B. Simpson, M. J. Padgett, and L. Allen, Phys. Rev. A **54**, R3742 (1996).  
 [9] J. Courtial, K. Dholakia, L. Allen, and M. J. Padgett, Phys. Rev. A **56**, 4193 (1997).  
 [10] J. Arlt, K. Dholakia, L. Allen, and M. J. Padgett, Phys. Rev. A **59**, 3950 (1999).  
 [11] A. Mair, A. Vaziri, G. Weihs, and A. Zeilinger, Nature (London) **412**, 313 (2001).  
 [12] D. P. Caetano, M. P. Almeida, P. H. Souto Ribeiro, J. A. O. Huguenin, B. Coutinho dos Santos, and A. Z. Khoury, Phys. Rev. A **66**, 041801(R) (2002).  
 [13] A. Gatti and L. A. Lugiato, Phys. Rev. A **52**, 1675 (1995).  
 [14] L. A. Lugiato and A. Gatti, Phys. Rev. Lett. **70**, 3868 (1993).  
 [15] M. Marte, H. Ritsch, K. I. Petsas, A. Gatti, L. A. Lugiato, C. Fabre, and D. Leduc, Opt. Express **3**, 71 (1998).  
 [16] L. A. Lugiato and I. Marzoli, Phys. Rev. A **52**, 4886 (1995).  
 [17] L. A. Lugiato and Ph. Grangier, J. Opt. Soc. Am. B **14**, 225 (1997).  
 [18] M. Vaupel, A. Maître, and C. Fabre, Phys. Rev. Lett. **83**, 5278 (1999).  
 [19] S. Ducci, N. Treps, A. Maître, and C. Fabre, Phys. Rev. A **64**, 023803 (2001).  
 [20] P. Suret, D. Derozier, M. Lefranc, J. Zemmouri, and S. Bielawski, J. Opt. Soc. Am. B **19**, 395 (2002).  
 [21] A. V. Mamaev, M. Saffman, and A. A. Zozulya, Phys. Rev. Lett. **77**, 4544 (1996).  
 [22] Gabriel Molina-Terriza, Lluís Torner, and Dmitri V. Petrov, Opt. Lett. **24**, 899 (1999).  
 [23] B. Boulanger, I. Rousseau, J. P. Fve, M. Maglione, B. Mnaert,

- and G. Marnier, *IEEE J. Quantum Electron.* **35**, 281 (1999).
- [24] Dmitri V. Petrov, Fernando Canal, and Lluis Torner, *Opt. Commun.* **143**, 265 (1997).
- [25] T. Debuisschert, A. Sizmann, E. Giacobino, and C. Fabre, *J. Opt. Soc. Am. B* **10**, 1668 (1993).
- [26] M. J. Padgett and J. Courtial, *Opt. Lett.* **24**, 430 (1999).
- [27] Antony E. Siegman, *Lasers* (University Science Books, Sausalito, California, 1986).
- [28] C. Schwob, P. F. Cohadon, C. Fabre, M. A. M. Marte, H. Ritsch, A. Gatti, and L. Lugiato, *Appl. Phys. B: Lasers Opt.* **66**, 685 (1998).
- [29] M. K. Olsen, K. Dechoum, and L. I. Plimak, *Opt. Commun.* **223**, 123 (2003).
- [30] M. K. Olsen, L. I. Plimak, and A. Z. Khoury, *Opt. Commun.* **215**, 101 (2003).
- [31] P. Drummond, K. Dechoum, and S. Chaturvedi, *Phys. Rev. A* **65**, 033806 (2002).
- [32] V. G. Dmitriev, G. G. Gurzadyan, and D. N. Nikogosyan, *Handbook of Nonlinear Optical Crystals*, Springer Series in Optical Sciences, Vol. 64 (Springer-Verlag, Berlin, 1991)
- [33] A. Yariv, *Quantum Electronics* (Wiley, New York, 1988).
- [34] R. Martínez-Herrero, J. M. Movilla, and P. M. Mejías, *J. Opt. Soc. Am. A* **18**, 2009 (2001).
- [35] Alessandro Ciattoni, Gasbriella Cincotti, Damiano Provenziani, and Claudio Palma, *Phys. Rev. E* **66**, 036614 (2002).
- [36] J. A. Fleck and M. D. Feit, *J. Opt. Soc. Am.* **73**, 920 (1983).